Symbolic-Numerical Solution of Boundary-Value Problems with Self-adjoint Second-Order Differential Equation Using the Finite Element Method with Interpolation Hermite Polynomials

Alexander A. Gusev[1], Ochbadrakh Chuluunbaatar[1,2], Sergue I. Vinitsky[1], Vladimir L. Derbov[3], Andrzej Góźdź[4], Luong Le Hai[1,5], and Vitaly A. Rostovtsev[1]

[1] Joint Institute for Nuclear Research, Dubna, Russia, gooseff@jinr.ru
[2] National University of Mongolia, UlaanBaatar, Mongolia
[3] Saratov State University, Saratov, Russia
[4] Institute of Physics, Maria Curie-Skłodowska University, Lublin, Poland
[5] Belgorod State University, Belgorod, Russia

Abstract. We present a symbolic algorithm generating finite-element schemes with interpolating Hermite polynomials intended for solving the boundary-value problems with self-adjoint second-order differential equation and implemented in the Maple computer algebra system. Recurrence relations for the calculation in analytical form of the interpolating Hermite polynomials with nodes of arbitrary multiplicity are derived. The integrals of interpolating Hermite polynomials are used for constructing the stiffness and mass matrices and formulating a generalized algebraic eigenvalue problem. The algorithm is used to generate Fortran routines that allow solution of the generalized algebraic eigenvalue problem with matrices of large dimension. The efficiency of the programs generated in Maple and Fortran is demonstrated by the examples of exactly solvable quantum-mechanical problems with continuous and piecewise continuous potentials.

1 Introduction

The study of mathematical models that describe tunneling and channeling of composite quantum systems through multidimensional barriers, photo-ionization and photo-absorption in molecular, atomic, nuclear, and quantum-dimensional semiconductor systems, requires high-accuracy efficient algorithms and programs for solving boundary-value problems (BVPs) [7,5,8,9,13].

In this direction, using the variation-projection BVP formulation and finite element method (FEM) with Lagrange interpolation elements [12,2,1], the symbolic-numeric algorithms (SNAs) and programs have been elaborated [5,6,4]. This implementation of FEM using the interpolation Lagrange polynomials (ILPs) was such that it preserved only the continuity of the solution itself in

V.P. Gerdt et al. (Eds.): CASC Workshop 2014, LNCS 8660, pp. 138–154, 2014.

the course of its numerical approximation on a finite-element grid. However, in the above class of problems, particularly, in quantum-dimensional semiconductor systems, the continuity should be preserved not only for the solution (wave function) itself, but also for the probability current [2,10]. The required continuity of the solution derivatives can be preserved in FEM numerical approximation using the interpolation Hermite polynomials (IHPs) [3,11].

This motivated the aim of the present work, namely, the use of FEM with IHPs to elaborate SNAs implemented in Maple-Fortran for the solution of the BVPs with self-adjoint second order differential equation, and the analysis of the approximate numerical solutions in benchmark calculations.

In this paper, we present a symbolic algorithm implemented in Maple computer algebra system (CAS) that generates finite-element calculation schemes for solving BVPs for the self-adjoint second-order differential equation using interpolating Hermite polynomials. We derived recurrence relations for the calculation of the IHPs with nodes of arbitrary multiplicity. The stiffness and mass matrices are expressed via the integrals of products of the BVP coefficient functions, the IHPs and their derivatives. The result is used to formulate a generalized algebraic eigenvalue problem solved in Maple for matrices of small dimension. We use the symbolic algorithm to generate Fortran routines that allow the solution of the generalized algebraic eigenvalue problem with matrices of large dimension. We demonstrate the efficiency of the programs generated in Maple and Fortran for 100×100 and higher-order matrices, respectively, in benchmark calculations for exactly solvable quantum-mechanical problems with continuous and piecewise continuous potentials.

The paper is organized as follows. In Section 2, the formulation of BVPs and variational functional is presented. Section 3 describes the algorithm that generates algebraic problems using the finite element method with interpolation Hermite polynomials. In Section 4, the benchmark calculations are analysed. The obtained results and further development of SNA are discussed in Conclusion.

2 Formulation of BVPs

We consider a self-adjoint second-order differential equation with respect to the unknown solution $\Phi(z)$ in the region $z \in \Omega_z = (z^{\min}, z^{\max})$ [4]

$$(D - 2E)\,\Phi(z) = 0, \quad D = -\frac{1}{f_1(z)}\frac{\partial}{\partial z} f_2(z) \frac{\partial}{\partial z} + V(z). \tag{1}$$

If no additional restrictions are explicitly specified, we assume $f_1(z) > 0$, $f_2(z) > 0$, and $V(z)$ to be continuous functions that have derivatives up to the order of $\kappa^{\max} \geq 1$ in the domain $z \in \bar{\Omega}_z = [z^{\min}, z^{\max}]$. In quantum mechanics, Eq. (1) is actually the Schrödinger equation that describes a particle with the wave function $\Phi(z)$ and the energy E.

For a discrete-spectrum problem, the eigenfunctions $\Phi(z) = \Phi_m(z) \in \mathcal{H}_2^2$ in the Sobolev space $\mathcal{H}_2^2$ corresponding to the eigenvalues $E_1 < E_2 < \ldots < E_m <$

... are to satisfy the boundary condition of the first (I) and/or the second (II) and/or the third (III) kind at given values of parameters $\mathcal{R}(z^t)$

$$\text{(I)}: \quad \Phi_m(z^t) = 0, \quad t = \min \text{ and/or } \max, \tag{2}$$

$$\text{(II)}: \quad f_1(z)\frac{d\Phi_m(z)}{dz}\Big|_{z=z^t} = 0, \quad t = \min \text{ and/or } \max, \tag{3}$$

$$\text{(III)}: \quad \frac{d\Phi_m(z)}{dz}\Big|_{z=z^t} = \mathcal{R}(z^t)\Phi_m(z^t), \quad t = \min \text{ and/or } \max \tag{4}$$

along with the normalization and orthogonality condition

$$\langle \Phi_m(z)|\Phi_{m'}(z)\rangle = \int_{z^{\min}}^{z^{\max}} f_1(z)(\Phi_m(z))^*\Phi_{m'}(z)dz = \delta_{mm'}. \tag{5}$$

The solution of the above BPVs can be reduced to the calculation of stationary points of a variational functional [12,6]

$$\Xi(\Phi, E, z^{\min}, z^{\max}) \equiv \int_{z^{\min}}^{z^{\max}} \Phi^*(z)\,(D - 2E)\,\Phi(z)dz = \Pi(\Phi, E, z^{\min}, z^{\max})$$
$$-f_2(z^{\max})\Phi^*(z^{\max})\mathcal{R}(z^{\max})\Phi(z^{\max}) + f_2(z^{\min})\Phi^*(z^{\min})\mathcal{R}(z^{\min})\Phi(z^{\min}), \tag{6}$$

where the symmetric functional $\Pi(\Phi, E, z^{\min}, z^{\max})$ is expressed as

$$\Pi(\Phi, E, z^{\min}, z^{\max}) = \int_{z^{\min}}^{z^{\max}} \Big[f_2(z)\frac{d\Phi^*(z)}{dz}\frac{d\Phi(z)}{dz} + f_1(z)\Phi^*(z)V(z)\Phi(z) \tag{7}$$
$$-f_1(z)2E\Phi^*(z)\Phi(z)\Big]dz.$$

Here $\mathcal{R}(z) \to \infty$ and $\mathcal{R}(z) = 0$ for discrete spectrum problem with BCs (I) and BCs (II), Eqs. (2) and (3), respectively.

3 FEM Generation of Algebraic Problems

High-accuracy computational schemes for solving the BVP (1)–(4) can be derived from the variational functional (6), (7) basing on the FEM. The general idea of the FEM in one-dimensional space is to divide the interval $[z^{\min}, z^{\max}]$ into many small domains referred to as elements. The size of the elements can be defined free enough to account for physical properties or qualitative behavior of the desired solutions, such as smoothness.

The interval $\Delta = [z^{\min}, z^{\max}]$ is covered by a set of n elements $\Delta_j = [z_j^{\min}, z_j^{\max} \equiv z_{j+1}^{\min}]$ in such a way that $\Delta = \bigcup_{j=1}^{n} \Delta_j$. Thus, we obtain the grid

$$\Omega^{h_j(z)}[z^{\min}, z^{\max}] = \{z^{\min} = z_1^{\min}, z_j^{\max} = z_j^{\min} + h_j, j = 1, \ldots, n-1, \tag{8}$$
$$z_n^{\max} = z_n^{\min} + h_n = z^{\max}\},$$

where $z_j^{\min} \equiv z_{j-1}^{\max}$, $j = 2, \ldots, n$ are the mesh points, and the steps $h_j = z_j^{\max} - z_j^{\min}$ are the lengths of the elements Δ_j.

3.1 Interpolation Hermite Polynomials

In each element Δ_j we define the equidistant sub-grid $\Omega_j^{h_j(z)}[z_j^{\min}, z_j^{\max}] = \{z_{(j-1)p} = z_j^{\min}, z_{(j-1)p+r}, r = 1, \ldots, p-1, z_{jp} = z_j^{\max}\}$ with the nodal points $z_r \equiv z_{(j-1)p+r}$ determined by the formula

$$z_{(j-1)p+r} = ((p-r)z_j^{\min} + rz_j^{\max})/p, \quad r = 0, \ldots, p. \tag{9}$$

As a set of basis functions $\{N_l(z, z_j^{\min}, z_j^{\max})\}_{l=0}^{l^{\max}}$, $l^{\max} = \sum_{r=0}^{p} \kappa_r^{\max}$ we will use the IHPs $\{\{\varphi_r^{\kappa}(z)\}_{r=0}^{p}\}_{\kappa=0}^{\kappa_r^{\max}-1}$ in the nodes z_r, $r = 0, \ldots, p$ of the grid (9). The values of the functions $\varphi_r^{\kappa}(z)$ with their derivatives up to the order $(\kappa_r^{\max} - 1)$, i.e. $\kappa = 0, \ldots, \kappa_r^{\max} - 1$, where $\kappa_r^{\max}$ is referred to as the multiplicity of the node z_r, are determined by the expressions [3]

$$\varphi_r^{\kappa}(z_{r'}) = \delta_{rr'}\delta_{\kappa 0}, \quad \left.\frac{d^{\kappa'}\varphi_r^{\kappa}(z)}{dz^{\kappa'}}\right|_{z=z_{r'}} = \delta_{rr'}\delta_{\kappa\kappa'}. \tag{10}$$

To calculate the IHPs we introduce the auxiliary weight function

$$w_r(z) = \prod_{r'=0, r' \neq r}^{p} \left(\frac{z - z_{r'}}{z_r - z_{r'}}\right)^{\kappa_{r'}^{\max}}, \qquad w_r(z_r) = 1. \tag{11}$$

The weight function derivatives can be presented as a product

$$\frac{d^{\kappa} w_r(z)}{dz^{\kappa}} = w_r(z) g_r^{\kappa}(z),$$

where the factor $g_r^{\kappa}(z)$ is calculated by means of the recurrence relations

$$g_r^{\kappa}(z) = \frac{dg_r^{\kappa-1}(z)}{dz} + g_r^1(z) g_r^{\kappa-1}(z), \tag{12}$$

with the initial conditions

$$g_r^0(z) = 1, \quad g_r^1(z) \equiv \frac{1}{w_r(z)} \frac{dw_r(z)}{dz} = \sum_{r'=0, r' \neq r}^{p} \frac{\kappa_{r'}^{\max}}{z - z_{r'}}.$$

We will seek for the IHPs $\varphi_r^{\kappa}(z)$ in the following form:

$$\varphi_r^{\kappa}(z) = w_r(z) \sum_{\kappa'=0}^{\kappa_r^{\max}-1} a_r^{\kappa,\kappa'} (z - z_r)^{\kappa'}. \tag{13}$$

Differentiating the function (13) by z at the point of z_r and using Eq. (11), we obtain

$$\left.\frac{d^{\kappa'}\varphi_r^{\kappa}(z)}{dz^{\kappa'}}\right|_{z=z_r} = \sum_{\kappa''=0}^{\kappa'} \frac{\kappa'!}{\kappa''!(\kappa' - \kappa'')!} g_r^{\kappa'-\kappa''}(z_r) a_r^{\kappa,\kappa''} \kappa''!. \tag{14}$$

Hence we arrive at the expression for the coefficients $a_r^{\kappa,\kappa'}$

$$a_r^{\kappa,\kappa'} = \left(\left. \frac{d^{\kappa'} \varphi_r^{\kappa}(z)}{dz^{\kappa'}} \right|_{z=z_r} - \sum_{\kappa''=0}^{\kappa'-1} \frac{\kappa'!}{\kappa''!(\kappa'-\kappa'')!} g_r^{\kappa'-\kappa''}(z_r) a_r^{\kappa,\kappa''} \kappa''! \right) / \kappa'!. \quad (15)$$

Taking Eq. (10) into account, we finally get:

$$a_r^{\kappa,\kappa'} = \begin{cases} 0, & \kappa' < \kappa, \\ 1/\kappa'!, & \kappa' = \kappa, \\ -\sum\limits_{\kappa''=\kappa}^{\kappa'-1} \frac{1}{(\kappa'-\kappa'')!} g_r^{\kappa'-\kappa''}(z_r) a_r^{\kappa,\kappa''}, & \kappa' > \kappa. \end{cases}$$

Note that all degrees of interpolation Hermite polynomials $\varphi_r^{\kappa}(z)$ do not depend on κ and equal $p' = \sum_{r'=0}^{p} \kappa_r^{\max} - 1$. Below we consider only the IHPs with the nodes of identical multiplicity $\kappa_r^{\max} = \kappa^{\max}$, $r = 0, \ldots, p$. In this case, the degree of the polynomials is equal to $p' = \kappa^{\max}(p+1) - 1$. We introduce the following notation for such polynomials:

$$N_{\kappa^{\max} r + \kappa}(z, z_j^{\min}, z_j^{\max}) = \varphi_r^{\kappa}(z), \quad r = 0, \ldots, p, \quad \kappa = 0, \ldots, \kappa^{\max} - 1. \quad (16)$$

These IHPs form a basis in the space of polynomials having the degree $p' = \kappa^{\max}(p+1) - 1$ in the element $z \in [z_j^{\min}, z_j^{\max}]$ that have continuous derivatives up to the order $\kappa^{\max} - 1$ at the boundary points $z_j^{\min}$ and $z_j^{\max}$ of the element $z \in [z_j^{\min}, z_j^{\max}]$. The IHPs at $\kappa^{\max} = 1, 2, 3$ and $p = 4$ are shown in Fig. 1. It is seen that the values of IHP $N_{\kappa^{\max} p + \kappa}(z, z_j^{\min}, z_j^{\max})$ and $N_{\kappa}(z, z_{j+1}^{\min}, z_{j+1}^{\max})$ (at $r = p$ and $r = 0$) and their derivatives up to the order $\kappa^{\max} - 1$ coincide at the mutual point $z_j^{\max} = z_{j+1}^{\min}$ of the adjacent elements. Moreover, the boundary points are nodes (zeros) of multiplicity $\kappa^{\max}$ of other IHPs, irrespective of the length of elements of $[z_j^{\min}, z_j^{\max}]$ and $[z_{j+1}^{\min}, z_{j+1}^{\max}]$. This allows construction of a basis of piecewise and polynomial functions having continuous derivatives to the order of $\kappa^{\max} - 1$ in any set $\Delta = \bigcup_{j=1}^{n} \Delta_j = [z_j^{\min}, z_j^{\max}]$ of elements $\Delta_j = [z_j^{\min}, z_j^{\max} \equiv z_{j+1}^{\min}]$. The **Algorithm 1** of the IHP construction is presented in Appendix A and implemented in the CAS Maple.

3.2 Generation of Algebraic Eigenvalue Problems

We consider a discrete representation of the solutions $\Phi(z)$ of the problem (1), (5), (4) reduced by means of the FEM to the variational functional (6), (7) on the finite-element grid,

$$\Omega_{h_j(z)}^{p}[z^{\min}, z^{\max}] = [z_0 = z^{\min}, z_l, l = 1, \ldots, np-1, z_{np} = z^{\max}],$$

with the mesh points $z_l = z_{jp} = z_j^{\max} \equiv z_{j+1}^{\min}$ of the grid $\Omega^{h_j(z)}[z^{\min}, z^{\max}]$ determined by Eq. (8) and the nodal points $z_l = z_{(j-1)p+r}$, $r = 0, \ldots, p$ of the sub-grids $\Omega_j^{h_j(z)}[z_j^{\min}, z_j^{\max}]$, $j = 1, \ldots, n$, determined by Eq. (9). The solutions

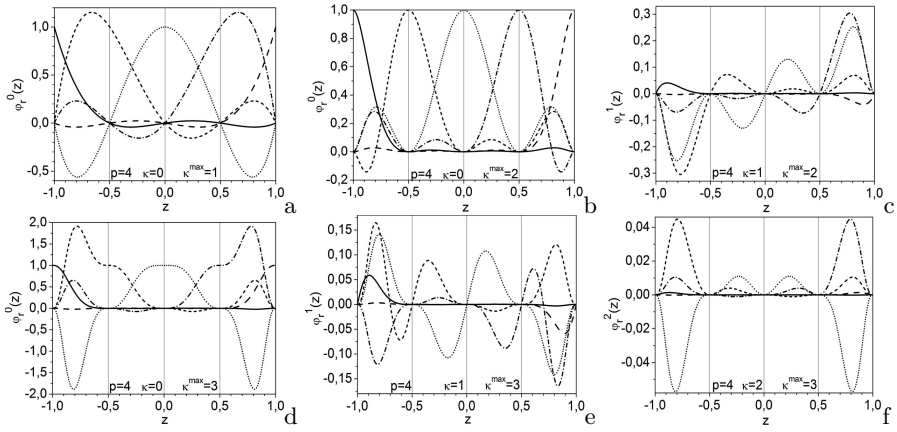

Fig. 1. The IHP coinciding at $\kappa^{\max} = 1$ with the ILP (a) and IHPs at $\kappa^{\max}$ =2 (b, c) and $\kappa^{\max}$ =3 (d, e, f). Here $p + 1 = 5$ is the number of nodes in the subinterval, $\Delta_j = [z_j^{\min} = -1, z_j^{\max} = 1]$. The grid nodes z_r are shown by vertical lines.

$\Phi^h(z) \approx \Phi(z)$ are sought for in the form of a finite sum over the basis of local functions $N_\mu^g(z)$ at each nodal point $z = z_k$ of the grid $\Omega^p_{h_j(z)}[z^{\min}, z^{\max}]$:

$$\Phi^h(z) = \sum_{\mu=0}^{L-1} \Phi^h_\mu N^g_\mu(z), \quad \Phi^h(z_l) = \Phi^h_{l\kappa^{\max}}, \quad \left.\frac{d^\kappa \Phi^h(z)}{dz^\kappa}\right|_{z=z_l} = \Phi^h_{l\kappa^{\max}+\kappa} \quad (17)$$

where $L = (pn+1)\kappa^{\max}$ is the number of local functions and Φ^h_μ at $\mu = l\kappa^{\max}+\kappa$ are the nodal values of the κth derivatives of the function $\Phi^h(z)$ (including the function $\Phi^h(z)$ itself for $\kappa = 0$) at the points z_l.

The local functions $N^g_\mu(z) \equiv N^g_{l\kappa^{\max}+\kappa}(z)$ are piecewise polynomials of the given order p', their derivative of the order κ at the node z_l equals one, and the derivative of the order $\kappa' \neq \kappa$ at this node equals zero, while the values of the function $N^g_\mu(z)$ with all its derivatives up to the order $(\kappa^{\max} - 1)$ equal zero at all other nodes $z_{l'} \neq z_l$ of the grid $\Omega_{h_j(z)}$, i.e., $\left.\frac{d^\kappa N_{l'\kappa^{\max}+\kappa'}}{dz^\kappa}\right|_{z=z_l} = \delta_{ll'}\delta_{\kappa\kappa'}$, $l = 0, \ldots, np$, $\kappa = 0, \ldots, \kappa^{\max} - 1$.

For the nodes z_l of the grid that do not coincide with the mesh points $z_j^{\max}$, i.e., at $l \neq jp$, $j = 1 \ldots n-1$, the polynomial N^g_μ at $\mu = ((j-1)p + r)\kappa^{\max} + \kappa$ has the form

$$N^g_{(p(j-1)+r)\kappa^{\max}+\kappa} = \begin{cases} N_{\kappa^{\max}r+\kappa}(z, z_j^{\min}, z_j^{\max}), & z \in \Delta_j; \\ 0, & z \notin \Delta_j, \end{cases} \quad (18)$$

i.e., it is defined as the IHP $N_{\kappa^{\max}r+\kappa}(z, z_j^{\min}, z_j^{\max})$ in the interval $z \in \Delta_j$ and zero otherwise. Since the points $z_j^{\min}$ and $z_j^{\max}$ are nodes of multiplicity $\kappa^{\max}$, such piecewise polynomial functions and their derivatives up to the order $\kappa^{\max}-1$

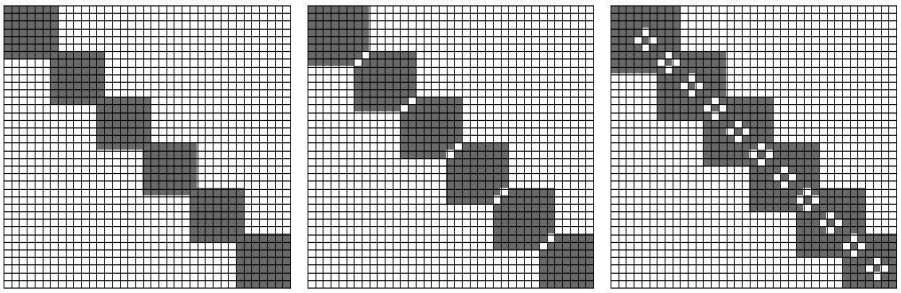

Fig. 2. The structure of matrices $B_{L_1L_2}$ and $A_{L_1L_2}$ for the potential $V(z) = 0$, the number of elements $n = 6$ in the entire interval $(z^{\min}, z^{\max})$, and different values of the multiplicity of nodes $\kappa^{\max}$ and the number of subintervals p. From left to right: $(\kappa^{\max}, p) = (1, 6)$, $(\kappa^{\max}, p) = (2, 3)$, $(\kappa^{\max}, p) = (3, 2)$. The dimensions of matrices are $L \times L$, $L = \kappa^{\max}(np + 1)$: 37×37, 38×38, 39×39.

are continuous in the entire interval Δ. In Fig. 1 such IHPs are plotted by dotted, short-dashed and dot-dashed lines.

For the nodal points of the grid z_l that coincide with one of the mesh points $z_j^{\max}$ belonging to two elements Δ_j and Δ_{j+1}, $j = 1 \dots n-1$, i.e., for $l = jp$, the polynomial, whose derivative of the order κ equals one at the node z_l, has the form

$$N^g_{p\kappa^{\max}j+\kappa} = \begin{cases} N_{\kappa^{\max}p+\kappa}(z, z_j^{\min}, z_j^{\max}), & z \in \Delta_j; \\ N_\kappa(z, z_{j+1}^{\min}, z_{j+1}^{\max}), & z \in \Delta_{j+1}; \\ 0, & z \notin \Delta_j \cup \Delta_{j+1}, \end{cases} \tag{19}$$

In other words, it is constructed by joining the polynomial $N_{p\kappa^{\max}+\kappa}(z, z_j^{\min}, z_j^{\max})$ defined in the element Δ_j with the polynomial $N_\kappa(z, z_{j+1}^{\min}, z_{j+1}^{\max})$ defined in the element Δ_{j+1}. This polynomial is also continuous with all its derivatives of the order $\kappa^{\max} - 1$ in the interval $z \in \Delta$. The corresponding IHPs are plotted in Fig. 1 by solid and long-dashed lines.

The substitution of the expansion (17) into the variational functional (6), (7) reduces the solution of the problem (1)–(5) to the solution of the generalized algebraic eigenvalue problem with respect to the desired set of eigenvalues E and eigenvectors $\boldsymbol{\Phi}^h = \{\Phi_\mu^h\}_{\mu=0}^{L-1}$:

$$(\tilde{\mathbf{A}} - 2E\,\mathbf{B})\boldsymbol{\Phi}^h = 0. \tag{20}$$

Here $\tilde{\mathbf{A}} = \mathbf{A} + \mathbf{M}_{\min} - \mathbf{M}_{\max}$ and $\mathbf{B}$ are symmetric $L \times L$ stiffness and mass matrices, $L = \kappa^{\max}(np+1)$, $\mathbf{M}_{\max}$ and $\mathbf{M}_{\min}$ are $L \times L$ matrices with zero elements except $M_{11} = f_2(z^{\min})R(z^{\min})$ and $M_{L+1-\kappa^{\max},L+1-\kappa^{\max}} = f_2(z^{\max})R(z^{\max})$, respectively. The **Algorithm 2** that generates the local functions $N_\mu^g(z)$ defined by (18), (19) and the matrices $\mathbf{A}$ and $\mathbf{B}$ is described in Appendix B and implemented in the CAS Maple.

Table 1. Runge coefficients (24) for the eigenvalues (Runge Eigv) and the eigenfunction (Runge EigF) of the first three lower-energy states calculated for schemes with different $\kappa^{\max}$ and p up to order $p' = \kappa^{\max}(p+1) - 1 = 8$ at $h = 0.125$ for schemes with $p' = 7$, $p' = 8$, and at $h = 0.0625$ for the rest of the schemes. Theoretical estimates of Runge coefficient for the convergence of eigenvalues and eigenfunctions are $2p'$ and $(p'+1)$, respectively. The execution time T_h (in seconds) for the mesh step $h = 1/32$ is presented in the last column.

$\kappa^{\max}$	p	p'	Runge Eigv			$2p'$	Runge EigF			$p'+1$	T_h
1	1	1	2.00	2.00	1.99	2	1.99	1.99	2.00	2	9.36
1	2	2	4.00	3.99	3.99	4	2.99	2.98	3.02	3	19.5
1	3	3	5.99	6.00	5.99	6	3.98	3.99	3.97	4	33.4
2	1	3	5.97	5.96	5.96	6	3.95	3.95	3.94	4	21.8
1	4	4	7.99	8.00	8.00	8	4.99	4.98	5.00	5	48.6
1	5	5	9.99	9.99	9.99	10	5.98	6.01	5.97	6	65.6
2	2	5	9.97	9.97	9.97	10	5.96	5.98	5.95	6	47.6
3	1	5	10.05	10.05	10.06	10	6.01	6.04	6.02	6	38.0
1	6	6	12.00	12.00	12.00	12	6.99	6.97	6.99	7	88.9
1	7	7	13.98	13.98	13.98	14	7.85	8.03	7.85	8	111.
2	3	7	13.88	13.87	13.87	14	7.77	7.95	7.77	8	82.3
4	1	7	13.59	13.58	13.57	14	7.61	7.57	7.59	8	59.6
1	8	8	16.13	16.00	15.99	16	9.00	8.82	9.09	9	139.
3	2	8	15.75	15.75	15.74	16	8.83	8.67	8.86	9	99.1

To solve equation (20) we have chosen the subspace iteration method [12,1] elaborated by Bathe [1] for the solution of large symmetric banded matrix eigenvalue problems. This method uses a skyline storage mode, which stores the components of the matrix column vectors within the nonzero band of the matrix and, therefore, is perfectly suitable for the banded FEM matrices. The procedure chooses a vector subspace of the full solution space and iterates upon the successive solutions in the subspace (for details, see [1]). Using the Rayleigh quotients for the eigenpairs, the iterations are repeated until the desired set of solutions in the iteration subspace converges to within the specified tolerance. Generally, 10–24 iterations are enough to converge the subspace to within the prescribed tolerance. If the matrix $\tilde{\mathbf{A}}$ in Eq. (20) is not positive-definite, the problem (20) is replaced with the following problem: $\check{\mathbf{A}}\boldsymbol{\Phi}^h = \check{E}^h\,\mathbf{B}\boldsymbol{\Phi}^h$, $\check{\mathbf{A}} = \tilde{\mathbf{A}} - \alpha\mathbf{B}$. The number α (the shift of the energy spectrum) is chosen such that the matrix $\check{\mathbf{A}}$ is positive-definite. The eigenvector of this problem is the same, and $E^h = \check{E}^h + \alpha$.

The theoretical estimate for the $\mathbf{H^0}$ norm of the difference between the exact solution $\Phi_m(z) \in \mathcal{H}_2^2$ and the numerical one $\Phi_m^h(z) \in \mathbf{H}^{\kappa^{\max}}$ has the order of

$$|E_m^h - E_m| \le c_1\, h^{2p'}, \quad \left\|\Phi_m^h(z) - \Phi_m(z)\right\|_0 \le c_2 h^{p'+1}, \tag{21}$$

where $h = \max_{1<j<n} h_j$ is the maximal step of the grid [12].

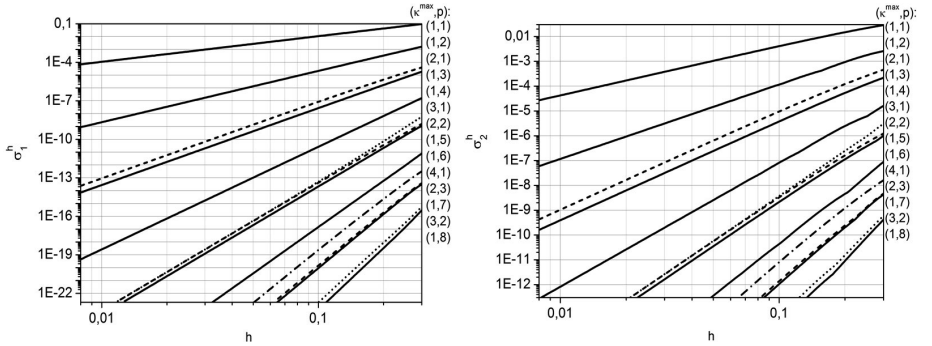

Fig. 3. Absolute errors $\sigma_1^h = |\varepsilon_1^{exact} - \varepsilon_1^h|$ and $\sigma_2^h = \max_{z\in\Omega^h(z)} |\chi_1^{exact}(z) - \chi_1^h(z)|$ for the ground state vs the grid step h calculated using approximation by IHPs with different $\kappa^{\max}$ and p

4 Benchmark Calculations

4.1 Modified Pöschl–Teller Potential

As an example, we consider the exactly solvable eigenvalue problem for Schrödinger equation in the units $\hbar = m = 1$:

$$\left(-\frac{d^2}{dz^2} + 2V(z) - 2E\right)\Phi(z) = 0, \tag{22}$$

with the modified Pöschl–Teller potential on the axis $z \in (-\infty, +\infty)$:

$$V(z) = -\frac{\alpha^2}{2}\frac{\lambda\,(\lambda-1)}{(\cosh(\alpha\,z))^2}, \tag{23}$$

where $\alpha > 0$ and $\lambda > 0$ are real-value parameters. The parameters $\lambda = 11/2$ and $\alpha = 1$ were chosen such that the discrete spectrum problem for Eq. (22) with the potential (23) had five eigenvalues $2E_m = [-20.25, -12.25, -6.25, -2.25, -0.25]$ with the corresponding five eigenfunctions $\psi_m(x)$ known in the analytical form.

The numerical experiments using the finite-element grid $\Omega^p_{h_j(z)}[z^{\min} = -40, z^{\max} = 40]$ demonstrated strict correspondence to the theoretical estimations (21) for eigenvalues and eigenfunctions. In particular, we calculated the Runge coefficients

$$\beta_l = \log_2\left|\frac{\sigma_l^h - \sigma_l^{h/2}}{\sigma_l^{h/2} - \sigma_l^{h/4}}\right|, \quad l = 1, 2, \tag{24}$$

on three twice condensed grids with the absolute errors

$$\sigma_1^h = |E_m^{exact} - E_m^h|, \quad \sigma_2^h = \max_{z\in\Omega^h(z)} |\Phi_m^{exact}(z) - \Phi_m^h(z)| \tag{25}$$

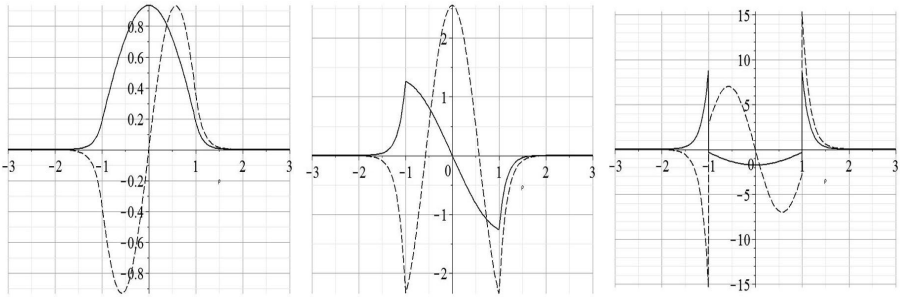

Fig. 4. The solutions and their first and second derivatives for the ground state (solid curves) and the first excited state (dashed curves) of the rectangular well potential problem

for the eigenvalues and eigenfunctions, respectively. From Eq. (25) we obtained the numerical estimations of the convergence order of the proposed numerical schemes, the theoretical estimates being $\beta_1 = 2p'$ and $\beta_2 = p' + 1$.

In Table 1, we show the Runge coefficients (24) for the eigenvalues (Runge Eigv) and the eigenfunction (Runge EigF) of the first three lower-energy states calculated for schemes with different $\kappa^{\max}$ and p up to order $p' = \kappa^{\max}(p+1)-1 = 8$. One can see that for the chosen $p' = 1 \div 8$, the numerical estimates of Runge coefficients lie within $2p' \pm 0.06$ for $p' = 1, \ldots, 6$ and $2p' \pm 0.56$ for $p' = 7, 8$ in the case of eigenvalues and within $(p' + 1) \pm 0.2$ in the case of eigenfunctions, which strongly corresponds to the theoretical error estimates (21). In Fig. 3, we show the dependence of absolute errors $\sigma_1^h = |\varepsilon_1^{exact} - \varepsilon_1^h|$ for eigenvalues and $\sigma_2^h = \max_{z \in \Omega^h(z)} |\chi_1^{exact}(z) - \chi_1^h(z)|$ for eigenfunctions of the ground state vs. the grid step h calculated using approximation by IHPs with different $\kappa^{\max}$ and p. In the double logarithmic scale, the errors lie on lines with different slopes that explicitly show the desirable order of approximation $p' = \kappa^{\max}(p + 1) - 1$ by IHPs with different $\kappa^{\max}$ and p.

For calculations, we used the program KANTBP 1.1 with the specified accuracy of $\sim 10^{-34}$ and the relative error tolerance of the eigenvalues $\epsilon_1 = 4 \cdot 10^{-34}$, implemented in Intel Fortran 77 on the computer 2 x Xeon 3.2 GHz, 4 GB RAM. The data type QUADRUPLE PRECISION provided 32 significant digits. The running time T_h for $h = 1/32 = 0.03125$ is presented in the last column of Table 1.

4.2 Rectangular Well Potential

For piecewise continuous potentials (or potentials with discontinuous derivatives), the approximation by IHPs does not converge to the desired solution with increasing number of nodes. Within the FEM approach, the following technique is used. Let the potential have the form $V(z) = \{V_i(z), z \in (\zeta_i^{\min}, \zeta_i^{\max})\}$, $\zeta_{i+1}^{\min} = \zeta_i^{\max}$, where $V_i(z)$ are $(p' + 1)$-times differentiable functions. The interval of the problem definition is divided into a set of subintervals $[z_j^{\min}, z_j^{\max}]$

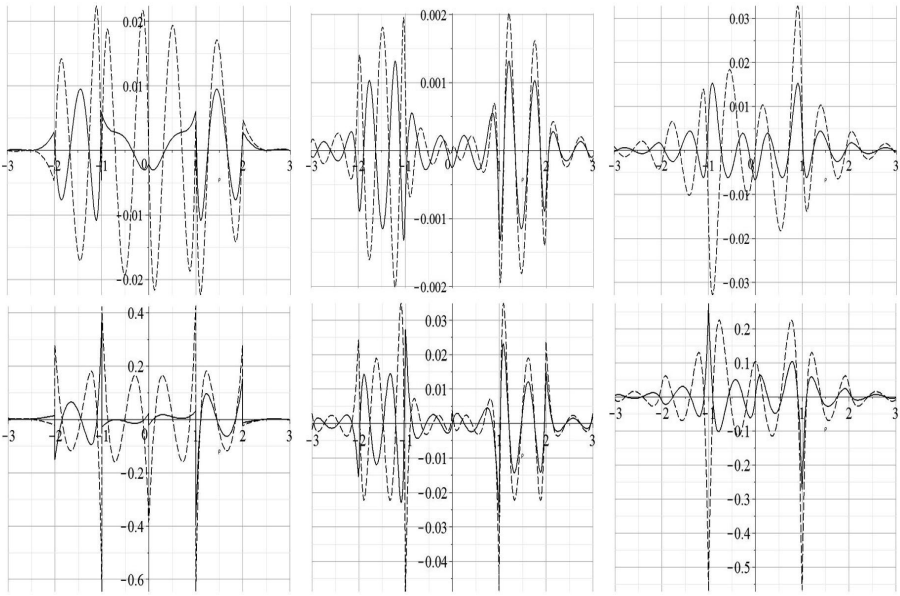

Fig. 5. The difference of numerical and exact eigenfunctions $D^{\kappa^{\max},p}_{swp,0} = \psi_0^{\kappa^{\max},p}(z) - \psi_0(z)$ (solid curves) and $D^{\kappa^{\max},p}_{swp,1} = \psi_1^{\kappa^{\max},p}(z) - \psi_1(z)$ (dashed curves) (upper panels) and their first derivatives (lower panels) for rectangular well potential for $n = 10$ elements in the interval $(-5, 5)$ and different values of the multiplicity of nodes $\kappa^{\max}$ and the number of subinterval divisions p. >From left to right: $(\kappa^{\max}, p) = (1, 3)$, $(\kappa^{\max}, p) = (2, 1)$, $(\kappa^{\max}, p) = (3, 1)$.

$(z_j^{\max} \equiv z_{j+1}^{\min})$, such that every point $\zeta_i^{\min}$, in which the second derivative of the solution is discontinuous, coincides with some boundary point $z_j^{\min}$.

Consider, e.g., the exactly solvable discrete-spectrum problem for Eq. (22) with the rectangular well potential $2V(z) = V_0$, if $|z| \leq a$, and $2V(z) = 0$ otherwise. At $a = 1$, $2V_0 = -50$ the discrete-spectrum problem has five eigenfunctions (see Fig. 4), expressed in the analytical form via five eigenvalues $2E_m = [-48.109146, -42.474904, -33.232792, -20.714111, -5.965365]$.

Since the first two eigenfunctions rapidly decrease, it is sufficient to use the finite-element grid $\Omega^p_{h_j(z)}[z^{\min} = -5, z^{\max} = 5]$. The calculation error for the first two eigenvalues is presented in Table 2. It is seen that the scheme with $\kappa^{\max} = 1$ and $\kappa^{\max} = 2$ having the same order of accuracy $p' = 3$ and $p' = 5$ $(p' = \kappa^{\max}(p + 1) - 1)$ yield nearly the same error (at $n = 20$, $h = 1/2$ the error is about 10^{-2} and $4 \cdot 10^{-6}$, respectively), while for $\kappa^{\max} = 3$, the error is much higher (about 10^{-2} at $n = 20$, $h = 1/2$). In Table 2, we show the Runge coefficients (24) for the eigenvalues of the first two lower-energy states calculated for schemes with different $\kappa^{\max}$ and p with order $p' = \kappa^{\max}(p + 1) - 1 = 3$ and $p' = \kappa^{\max}(p+1)-1 = 5$. One can see that for the chosen $p' = 3, 5$, the numerical estimates of Runge coefficients lie within $2p' \pm 0.5$ for schemes with $\kappa^{\max} = 1, 2$

Table 2. The absolute errors $\sigma_1^h(E_0)$ and $\sigma_1^h(E_1)$ of eigenvalues of ground and first exited state for square well potential for $a = 1$ and $2V_0 = -50$. The Runge coefficient (Ru) from (24) for the eigenvalues at $h = 1/4$, $n = 40$ and its theoretical estimates ($2p'$) are given in last two columns.

$(\kappa^{\max}, p)$	p'	$\sigma_1^{h=1}(E_0)$	$\sigma_1^{h=1/2}(E_0)$	$\sigma_1^{h=1/4}(E_0)$	$\sigma_1^{h=1/8}(E_0)$	$\sigma_1^{h=1/16}(E_0)$	Ru	$2p'$
(1,3)	3	1.93e-02	1.39e-03	4.44e-05	8.83e-07	1.48e-08	5.65	6
(2,1)	3	5.70e-02	3.15e-03	1.00e-04	2.21e-06	4.14e-08	5.50	6
(1,5)	5	2.47e-04	1.67e-06	3.82e-09	5.26e-12	2.22e-12	10.3	10
(2,2)	5	4.01e-04	2.59e-06	6.12e-09	8.59e-12	2.20e-13	9.51	10
(3,1)	5	1.48e-02	2.66e-03	3.51e-04	4.40e-05	5.50e-06	2.99	10
$(\kappa^{\max}, p)$	p'	$\sigma_1^{h=1}(E_1)$	$\sigma_1^{h=1/2}(E_1)$	$\sigma_1^{h=1/4}(E_1)$	$\sigma_1^{h=1/8}(E_1)$	$\sigma_1^{h=1/16}(E_1)$	Ru	$2p'$
(1,3)	3	9.96e-02	4.38e-03	1.25e-04	2.40e-06	3.96e-08	5.70	6
(2,1)	3	2.92e-01	1.14e-02	3.08e-04	6.33e-06	1.14e-07	5.60	6
(1,5)	5	6.44e-04	3.75e-06	7.93e-09	1.04e-11	2.63e-12	9.99	10
(2,2)	5	9.40e-04	5.66e-06	1.27e-08	1.74e-11	2.06e-13	9.53	10
(3,1)	5	6.70e-02	1.07e-02	1.39e-03	1.74e-04	2.17e-05	3.01	10

which strongly corresponds to the theoretical error estimates (21). While the scheme with $\kappa^{\max} = 3$, $p = 1$ of fifth order $p' = 5$ gives Runge coefficient $\beta_1 = 3$. Maximal discrepancies arise in the vicinities of discontinuity of the potential well (at $z = \pm 1$) because of a worse approximation of function with discontinuous second derivative by means of functions with continuous one.

It is due to the fact that the first derivative of the solution has a discontinuity at $z = \pm a$ displayed in Fig 4. To illustrate this fact, we display in Fig. 5 the discrepancies of eigenfunctions and their first derivatives. It is seen that the scheme with $\kappa^{\max} = 2$, $p = 1$ provides better approximation for eigenfunctions among schemes of third order $p' = 3$. The scheme of fifth order $p' = 5$ with $\kappa^{\max} = 3$, $p = 1$ leads to worse approximation in comparison with schemes of third order.

5 Conclusion

We presented the SNAs for solving the BVPs with self-adjoint second order differential equation using the FEM with interpolation Hermite polynomials. The proposed approach preserves the property of continuity of derivatives of the desired solutions. We demonstrated the efficiency of the programs generated in Maple and Fortran for 100×100 and greater-order matrices, respectively, in benchmark calculations for exactly solvable quantum-mechanical problems with continuous and piecewise continuous potentials. The analysis of approximate numerical solutions in benchmark calculations with smooth potentials shows

that the order $p' = \kappa^{\max}(p+1) - 1$ of the elaborated FEM schemes strongly corresponds to the theoretical error estimates. Schemes of higher order p' allow high-accuracy results at larger step of the finite-element grid, provided that the derivative of the p'th order is a smooth function. Schemes with the fixed order p' have similar rate convergence, the execution time being smaller for greater $\kappa^{\max}$ due to smaller dimension of matrices used in the calculations. However, if the κth derivative of the desired solution has discontinuity points, i.e., for potentials having a discontinuous derivative of the order $\kappa - 2$, the schemes with $\kappa^{\max} \geq \kappa$ operate worse, because in this case, the solution having discontinuous κ^{th}th derivatives is approximated by functions having no such discontinuities.

In future, the elaborated calculation schemes, algorithms, and programs will be applied to the analysis of models of molecular, atomic, and nuclear systems, as well as to quantum-dimensional systems such as quantum dots, wires, and wells in bulk semiconductors, and smooth irregular wave-guide structures with piecewise continuous potentials.

The authors thank Professor V.P. Gerdt for collaboration. The work was partially supported by the Russian Foundation for Basic Research (RFBR) (grants No. 14-01-00420 and 13-01-00668) and the Bogoliubov–Infeld program.

A Algorithm 1. Generation of IHPs

Input:
$z^{\min}, z^{\max}$, (formal parameters) the boundary points of the interval;
p is the number of subintervals: $p+1$ is the number of nodes of IHPs;
$\kappa^{\max}$ is the multiplicity of nodes;
$f_1(z)$ and $f_2(z)$ are coefficient functions from (1);
Output:
$N_{l_1}(z, z^{\min}, z^{\max})$ are IHPs, $l_1 = 0, \ldots, l_{\max}$, i.e. $l_{\max}+1$ is number of IHPs;
$A_{l_1;l_2}(z^{\min}, z^{\max})$ and $B_{l_1;l_2}(z^{\min}, z^{\max})$ are auxiliary integrals;
Local:
$l_{\max} = \kappa^{\max}(p+1) - 1$ is largest index of IHPs, $l_{\max}+1$ is number of IHPs;
z_r are nodes in subinterval;
$w_r(z)$ are weight functions;
$g_r^{\kappa}(z)$ are derivatives of order κ divided by weight function;
$a_r^{\kappa,\kappa'}$ are coefficients of expansion (13);

1: generation of IHPs and calculation of integrals in the interval $[z^{\min}, z^{\max}]$
1.1.: for r:=0 to p do
$z_r = ((p-r)z^{\min} + rz^{\max})/p$;
end for;
1.2.: for r:=0 to p do
1.2.1: auxiliary weight function
$w_r(z) = \prod_{r'=0, r' \neq r}^{p} \left(\frac{z - z_{r'}}{z_r - z_{r'}}\right)^{\kappa^{\max}}$;
1.2.2: recurrence relation for calculating the function $g_r^{\kappa}(z)$
$g_r^0(z) = 1$;

$g_r^1(z) = \sum_{r'=0, r' \neq r}^{p} \frac{\kappa^{\max}}{z - z_{r'}}$;
for κ:=2 to $\kappa^{\max} - 1$ do
$g_r^{\kappa}(z) = \frac{dg_r^{\kappa-1}(z)}{dz} + g_r^1(z) g_r^{\kappa-1}(z)$;
end for;

1.2.3: recurrence relation for calculation of coefficients $a_r^{\kappa,\kappa'}$
for κ:=0 to $\kappa^{\max} - 1$ do
$a_r^{\kappa,\kappa} = 1/\kappa'!$;
for κ':=$\kappa + 1$ to $\kappa^{\max} - 1$ do
$a_r^{\kappa,\kappa'} = -\sum_{\kappa''=\kappa}^{\kappa'-1} \frac{1}{(\kappa' - \kappa'')!} g_r^{\kappa' - \kappa''}(z_r) a_r^{\kappa,\kappa''}$;
end for;

1.2.4: calculation of IHP
$N_{\kappa^{\max} r + \kappa}(z, z^{\min}, z^{\max}) \equiv \varphi_r^{\kappa}(z) = w_r(z) \sum_{\kappa'=\kappa}^{\kappa^{\max}-1} a_r^{\kappa,\kappa'} (z - z_r)^{\kappa'}$;
end for;
end for;
$l_{\max} = \kappa^{\max}(p+1) - 1$;

1.3: calculation of the auxiliary integrals
for l_1:=0 to $l_{\max}$ do
for l_2:=l_1 to $l_{\max}$ do
$A_{l_1;l_2}(z^{\min}, z^{\max}) = \int_{z^{\min}}^{z^{\max}} f_2(z) \frac{dN_{l_1}(z, z^{\min}, z^{\max})}{dz} \frac{dN_{l_2}(z, z^{\min}, z^{\max})}{dz} dz$;
$B_{l_1;l_2}(z^{\min}, z^{\max}) = \int_{z^{\min}}^{z^{\max}} f_1(z) N_{l_1}(z, z^{\min}, z^{\max}) N_{l_2}(z, z^{\min}, z^{\max}) dz$;
end for;
end for;

Remarks. 1. In commonly used coordinates, the integrals in Step 1.3. are calculated analytically. If $f_1(z)$ or $f_2(z)$ are such that these integrals cannot be calculated analytically, then one can apply the expansion over the interpolation polynomials.

2. The auxiliary integrals $A_{l_1;l_2}(z^{\min}, z^{\max})$ and $B_{l_1;l_2}(z^{\min}, z^{\max})$ are symmetric with respect to permutations of their indexes.

B Algorithm 2: FEM Generation of Algebraic Eigenvalue Problem

Input:
n is the number of subintervals $\Delta_j = [z_j^{\min}, z_j^{\max} = z_j^{\min} + h_j]$;
$\Delta_j = [z_j^{\min}, z_j^{\max}]$ are sets of subintervals ($z_j^{\max} \equiv z_{j+1}^{\min}$);
p is the number of divisions of subintervals: $p+1$ is the number of nodes of IHP;
$\kappa^{\max}$ is the multiplicity of nodes;
$N_{l_1}(z, z^{\min}, z^{\max})$ are IHP;
$A_{l_1;l_2}(z^{\min}, z^{\max})$ and $B_{l_1;l_2}(z^{\min}, z^{\max})$ are auxiliary integrals from the **Algorithm 1**;
$V(z)$ is coefficient function from (1);

Output:
z_l are nodes in the whole interval, $l = 0, \ldots, np$;
N_l^g are piecewise polynomials;
$A_{L_1L_2}$ and $B_{L_1L_2}$ are matrices of algebraic eigenvalue problem (20);
Local:
$l_{\max} = \kappa^{\max}(p+1) - 1$ where $l_{\max} + 1$ is number of IHP;
$L = \kappa^{\max}(np+1)$ is the dimension of the algebraic eigenvalue problem.

2.1. calculation of grid points
  $z_0 = z_1^{\min}$;
  for $j := 1$ to n do
    for $r := 1$ to $p-1$ do
      $z_{(j-1)p+r} = ((p-r)z_j^{\min} + rz_j^{\max})/p$;
    end for;
    $z_{jp} = z_j^{\max}$;
  end for;
2.2. calculation of piecewise polynomials
  for $\kappa := 0$ to $\kappa^{\max} - 1$ do
    $N_\kappa^g = \{N_\kappa(z, z_1^{\min}, z_1^{\max}), z \in \Delta_1\}$;
    for $j := 1$ to n do
      for $r := 1$ to $p-1$ do
        $N^g_{((j-1)p+r)\kappa^{\max}+\kappa} = \{N_{\kappa^{\max}r+\kappa}(z, z_j^{\min}, z_j^{\max}), z \in \Delta_j; 0, z \notin \Delta_j\}$;
      end for;
      if $(j < n)$ then
        $N^g_{jp\kappa^{\max}+\kappa} := \{N_{\kappa^{\max}p+\kappa}(z, z_j^{\min}, z_j^{\max}), z \in \Delta_j;$
                $N_\kappa(z, z_{j+1}^{\min}, z_{j+1}^{\max}), z \in \Delta_{j+1}; 0, z \notin \Delta_j \cup \Delta_{j+1}\}$;
      else
        $N^g_{np\kappa^{\max}+\kappa} := \{N_{\kappa^{\max}p+\kappa}(z, z_n^{\min}, z_n^{\max}), z \in \Delta_n; 0, z \notin \Delta_n\}$;
      end if;
    end for;
  end for;
2.3. Generation of matrices **A** and **B**
  for $j := 1$ to n do
    for $l_1 := 0$ to $l_{\max} - 1$ do
      $L_1 = p\kappa^{\max}(j-1) + l_1 + 1$;
      for l_2 from l_1 to $l_{\max} - 1$ do
        $L_2 = p\kappa^{\max}(j-1) + l_2 + 1$;
        $A_{L_1L_2} = A_{L_1L_2} + A_{l_1;l_2}(z_j^{\min}, z_j^{\max})$
                $+ \int_{z_j^{\min}}^{z_j^{\max}} f_1(z)dz N_{L_1}(z, z_j^{\min}, z_j^{\max})V(z)N_{L_2}(z, z_j^{\min}, z_j^{\max})$;
        $B_{L_1L_2} = B_{L_1L_2} + B_{l_1;l_2}(z_j^{\min}, z_j^{\max})$;
  end for (j, l_1, l_2)

Remarks. 1. If the coefficients of the equation (1) are given in the tabular form, then we use the following matrix elements in Step 1.3 of Algorithm 1 and Step 2.3 of Algorithm 2:

$$\int_{z_j^{\min}}^{z_j^{\max}} f_1(z)dz N_{L_1}(z, z_j^{\min}, z_j^{\max}) V(z) N_{L_2}(z, z_j^{\min}, z_j^{\max}) = \sum_{r=0}^{p} \sum_{\kappa=0}^{\kappa_{\max}-1} V^{(\kappa)}(z_{(j-1)p+r}) V_{l_1;l_2;\kappa^{\max}r+\kappa}(z_j^{\min}, z_j^{\max})), \quad (26)$$

where $V_{l_1;l_2;l_3}(z^{\min}, z^{\max})$ are determined by integrals with IHPs

$$V_{l_1;l_2;l_3}(z_j^{\min}, z_j^{\max}) = \int_{z_j^{\min}}^{z_j^{\max}} f_1(z) N_{l_1}(z, z_j^{\min}, z_j^{\max}) \times N_{l_2}(z, z_j^{\min}, z_j^{\max}) N_{l_3}(z, z_j^{\min}, z_j^{\max}) dz. \quad (27)$$

The obtained expression will be exact for polynomial potentials of the degree smaller than p'. Generally this decomposition leads to numerical eigenfunctions and eigenvalues with the accuracy of order about $p'+1$. If the integrals in Step 1.3 of Algorithm 1 and Step 2.3 of Algorithm 2 cannot be calculated in the analytical form, then the Gauss integration rule [1,6] with $p'+1$ nodes is applied and held the theoretical estimations (21).

2. Using the local coordinate $\eta \in [-1, 1]$ related to the absolute coordinate z as $z = z_j^{\min} + h_j(1+\eta)/2$, $\frac{dz}{d\eta} = h_j/2$, one should exploit the following expansions of the function and its first derivative

$$\hat{\Phi}(z) = \sum_{r=0}^{p} \sum_{\kappa=0}^{\kappa^{\max}-1} \hat{\Phi}_{\kappa^{\max}r+\kappa} N_{\kappa^{\max}r+\kappa}(\eta, -1, 1) \left(\frac{dz}{d\eta}\right)^{\kappa},$$

$$\frac{d\hat{\Phi}(z)}{dz} = \sum_{r=0}^{p} \sum_{\kappa=0}^{\kappa^{\max}-1} \hat{\Phi}_{\kappa^{\max}r+\kappa} \frac{dN_{\kappa^{\max}r+\kappa}(\eta, -1, 1)}{d\eta} \left(\frac{dz}{d\eta}\right)^{\kappa-1}.$$

3. The matrices $A_{L_1L_2}$ and $B_{L_1L_2}$ are symmetric, their dimension is $L \times L$, where $L = \kappa^{\max}(np+1)$. They consist of n sub-matrices with the dimension $\kappa^{\max}(p+1) \times \kappa^{\max}(p+1)$. The intersections of these sub-matrices are blocks having the dimension $\kappa^{\max} \times \kappa^{\max}$. These blocks include elements that equal zero in both matrices $B_{L_1L_2}$ and $A_{L_1L_2}$ for $V(z) = 0$ and become nonzero in the matrix $A_{L_1L_2}$, when $V(z) \neq 0$. The existence of such elements is a manifestation of the IHPs symmetry. The total number of elements in all these blocks is $(n(p^2+2p)+1)(\kappa^{\max})^2$. Examples of banded matrix structures are shown in Fig. 2.

4. To impose the BC (III) in $z^{\min}$ one should apply $A_{11} = A_{11} + f_2(z^{\min})R(z^{\min})$, while to impose the BC (III) in $z^{\max}$ one should apply $A_{L+1-\kappa^{\max},L+1-\kappa^{\max}} = A_{L+1-\kappa^{\max},L+1-\kappa^{\max}} - f_2(z^{\max})R(z^{\max})$. To impose the BC (I) in $z^{\min}$ one should drop first row and first column, while to apply the BC (I) in $z^{\max}$ one should drop row and column with number $L+1-\kappa^{\max}$.

5. For small matrix dimensions ~ 100, the desired solution of the problem generated at Step 2.3 is performed using the built-in procedures of the Maple LinearAlgebra package. For large matrix dimensions $\sim 100 \div 1000000$, the subspace iteration method is used, implemented in the Fortran program SSPACE [1].

References

1. Bathe, K.J.: Finite Element Procedures in Engineering Analysis, Englewood Cliffs. Prentice Hall, New York (1982)
2. Becker, E.B., Carey, G.F., Tinsley Oden, J.: Finite elements. An introduction, vol. I. Prentice-Hall, Inc., Englewood Cliffs (1981)
3. Berezin, I.S., Zhidkov, N.P.: Computing Methods, vol. I. Pergamon Press, Oxford (1965)
4. Chuluunbaatar, O., Gusev, A.A., Vinitsky, S.I., Abrashkevich, A.G.: ODPEVP: A program for computing eigenvalues and eigenfunctions and their first derivatives with respect to the parameter of the parametric self-adjoined Sturm-Liouville problem. Comput. Phys. Commun. 180, 1358–1375 (2009)
5. Chuluunbaatar, O., Gusev, A.A., Gerdt, V.P., Kaschiev, M.S., Rostovtsev, V.A., Samoylov, V., Tupikova, T., Vinitsky, S.I.: A symbolic-numerical Algorithm for solving the eigenvalue problem for a hydrogen atom in the magnetic field: cylindrical coordinates. In: Ganzha, V.G., Mayr, E.W., Vorozhtsov, E.V. (eds.) CASC 2007. LNCS, vol. 4770, pp. 118–133. Springer, Heidelberg (2007)
6. Chuluunbaatar, O., et al.: KANTBP: A program for computing energy levels, reaction matrix and radial wave functions in the coupled-channel hyperspherical adiabatic approach. Comput. Phys. Commun. 177, 649–675 (2007)
7. Cwiok, S., et al.: Single-particle energies, wave functions, quadrupole moments and g-factors in an axially deformed Woods-Saxon potential with applications to the two-centre-type nuclear problems. Comput. Phys. Communications 46, 379–399 (1987)
8. Gusev, A.A., Chuluunbaatar, O., Gerdt, V.P., Rostovtsev, V.A., Vinitsky, S.I., Derbov, V.L., Serov, V.V.: Symbolic-numeric algorithms for computer analysis of spheroidal quantum dot models. In: Gerdt, V.P., Koepf, W., Mayr, E.W., Vorozhtsov, E.V. (eds.) CASC 2010. LNCS, vol. 6244, pp. 106–122. Springer, Heidelberg (2010)
9. Gusev, A.A., Vinitsky, S.I., Chuluunbaatar, O., Gerdt, V.P., Rostovtsev, V.A.: Symbolic-numerical algorithms to solve the quantum tunneling problem for a coupled pair of ions. In: Gerdt, V.P., Koepf, W., Mayr, E.W., Vorozhtsov, E.V. (eds.) CASC 2011. LNCS, vol. 6885, pp. 175–191. Springer, Heidelberg (2011)
10. Ramdas Ram-Mohan, L.: Finite Element and Boundary Element Aplications in Quantum Mechanics. Oxford University Press, New York (2002)
11. Samarski, A.A., Gulin, A.V.: Numerical methods, Nauka, Moscow (1989) (in Russian)
12. Strang, G., Fix, G.J.: An Analysis of the Finite Element Method. Prentice-Hall, Englewood Cliffs (1973)
13. Vinitsky, S., Gusev, A., Chuluunbaatar, O., Rostovtsev, V., Le Hai, L., Derbov, V., Krassovitskiy, P.: Symbolic-numerical algorithm for generating cluster eigenfunctions: quantum tunneling of clusters through repulsive barriers. In: Gerdt, V.P., Koepf, W., Mayr, E.W., Vorozhtsov, E.V. (eds.) CASC 2013. LNCS, vol. 8136, pp. 427–442. Springer, Heidelberg (2013)